ELSEVIER

PII: S0032-3861(97)10316-0

Polymer Vol. 39 No. 19, pp. 4631–4638, 1998

0032-3861/98/$19.00+0.00

π-Shaped double-graft copolymers: effect of molecular architecture on morphology

Chin Lee[a], Samuel P. Gido[a,*], Yiannis Poulos[b], Nikos Hadjichristidis[b,c], Nora Beck Tan[d], Samuel F. Trevino[a,e] and Jimmy W. Mays[f]

[a]*Polymer Science and Engineering Department, M. Keck Electron Microscopy Laboratory, University of Massachusetts, Amherst, MA 01003, USA*
[b]*Department of Chemistry, University of Athens, Panepistimiopolis Zografou 15771, Athens, Greece*
[c]*Institute of Electronic Structure and Laser, 711 10 Heraklion, Crete, Greece*
[d]*Polymers Research Branch, U.S. Army Research Laboratory, APG, Gaithersburg, MD 211005-5069, USA*
[e]*Reactor Radiation Division, NIST, Gaithersburg, MD 20899, USA*
[f]*Department of Chemistry, University of Alabama at Birmingham, Birmingham, AL 35294, USA*
(Received 28 July 1997; revised 8 October 1997; accepted 21 October 1997)

The morphologies formed by block copolymers with a double-graft, π or (S,I)I′(S,I) architecture were investigated using transmission electron microscopy (TEM) and small angle neutron scattering (SANS). Here S and I represent blocks of polystyrene and polyisoprene, respectively. These materials were synthesized using anionic polymerization and chlorosilane linking, and they were characterized using size exclusion chromatography, membrane osmometry, and low-angle laser light scattering. This characterization work confirmed the desired molecular architectures and narrow molecular weight distributions. The results of morphological characterization indicate that one can understand complex grafting architectures by decomposing them into fundamental building blocks, which are taken as the component single-graft structures out of which the larger structure is constructed. We propose rules for dividing structures into these components, which we call *constituting block copolymers*. For the π double-graft architecture, the constituting block copolymer is an asymmetric single-graft block copolymer. The morphological behaviour of the more complex double-graft architecture is approximately equivalent to that of the constituting single-graft block copolymer. Through the use of the constituting block copolymers we map the experimentally determined morphological behaviour of eight materials with π architecture onto the morphology diagram calculated by Milner for *miktoarm* stars. As in our previous study of asymmetric single-graft block copolymers, the asymmetry of the graft location along the backbone requires a generalization of the molecular asymmetry parameter, ε, used in the calculated morphology diagram.

(Keywords: block copolymer; graft copolymer; morphology)

INTRODUCTION

We report on the morphology of a series of eight model, double-graft copolymers with a (S,I)I′(S,I) or π architecture, which consists of a polyisoprene (PI) connector (I′) with one polystyrene (PS) graft (S) and one PI graft (I) at both ends, as shown in *Figure 1a*. Alternatively, this structure can be thought of as a single PI backbone with two PS blocks grafted at equal distances from the two backbone ends. The working hypothesis of this study is that complex molecular architectures with two or more grafting (or branching) junction points can be understood morphologically by analogy to the behaviour of their fundamental building blocks. The fundamental unit of architecture will be defined and will be referred to as the *constituting block copolymer*. The *molecular asymmetry parameter* of this constituting block copolymer, which contains both the effects of molecular architecture and of conformational asymmetry between the two block materials, then dictates the morphological behaviour.

* To whom correspondence should be addressed

Most previous work on block copolymers has focused on linear molecular architectures. This focus was dictated by the lack of known synthetic routes to well-defined, near-monodisperse block copolymers with more complex architectures such as grafted materials, and star block copolymers. With the development of new synthetic methods[1–8], experimental studies on more complex architectures began to emerge; this, in turn, inspired new theoretical studies of the effect of molecular architecture on morphological behaviour. Both theory and experiment have demonstrated that the architecture of block copolymers is a controlling factor in morphological behaviour.

The general approach by which the constituting block copolymer is identified for a given molecular architecture is now considered. Assuming a lamellar morphology for simplicity, in AB linear diblock copolymers, each domain consists of two brushes grafted from two opposite interfaces as shown in *Figure 2a*. In the diblock, each A or B block has a free chain end located in the interior of an A or B domain. For more complex molecular architectures (those with multiblock or graft architectures), at least some blocks have

no free chain ends. For example, the B domains of ABA triblock copolymers contain no free chain ends, only *loops* (blocks with both ends grafted from the same interface) and *bridges* (blocks with each of the two ends grafted on a different one of the two opposite interfaces). Although bridges and loops have a significant effect on some material properties[9–11], their effect on the morphological behaviour decreases as the molecular weight of the block copolymers increases. For materials with sufficient molecular weight to exist in the strong segregation regime, the effect of bridge and loop connections on morphology is close to negligible[12]. That is, we can estimate the morphological behaviour of molecular architectures with multiple junction points by imaging all bridge and loop blocks to be cut in half. The single junction point molecular architectures into which the complex architecture is divided by this hypothetical cutting procedure are the constituting block copolymers. The architectures shown in *Figure 2*: symmetric ABA triblocks, $(AB)_n$ stars,…ABABAB… infinite multiblocks and cyclic AB block copolymers, all have linear molecules as their constituting block copolymers. For ABA the constituting block copolymer is A(1/2B); for the $(AB)_n$ star the constituting block copolymer is AB, and for both the infinite multiblock and the cyclic AB block copolymer the constituting block copolymer is (1/2A)(1/2B). The notation used to specify the constituting block copolymer architecture and composition, gives the A and B block lengths in terms of their fractions of the block lengths in the original architecture. Some recent theoretical[13–18] and experimental[17] studies have indicated that the morphologies of the block copolymer architectures in *Figure 2* asymptotically approach those of their constituting block copolymers as the molecular weights increase.

A graft architecture, as shown in *Figure 1b*, will have a nonlinear constituting block copolymer. The constituting block copolymer is a single-graft architecture which may also be thought of as a three-arm *mikto*arm star block copolymer. It has recently been demonstrated that the asymmetric molecular architecture of *mikto*arm stars leads to substantial shifts in the morphology *versus* volume fraction behaviour of the *mikto*arm stars with respect to their corresponding linear diblock copolymers with the same chemical composition and molecular weight[12,19–21]. Milner[22] calculated a morphological diagram, *Figure 3*, for A_nB_m *mikto*arm star molecules in the strong segregation limit. In this calculation, the asymmetry due to the difference in A and B arm numbers was lumped with the conformational asymmetry[23–25] inherent in the A and B polymer chains into one *molecular asymmetry factor*,

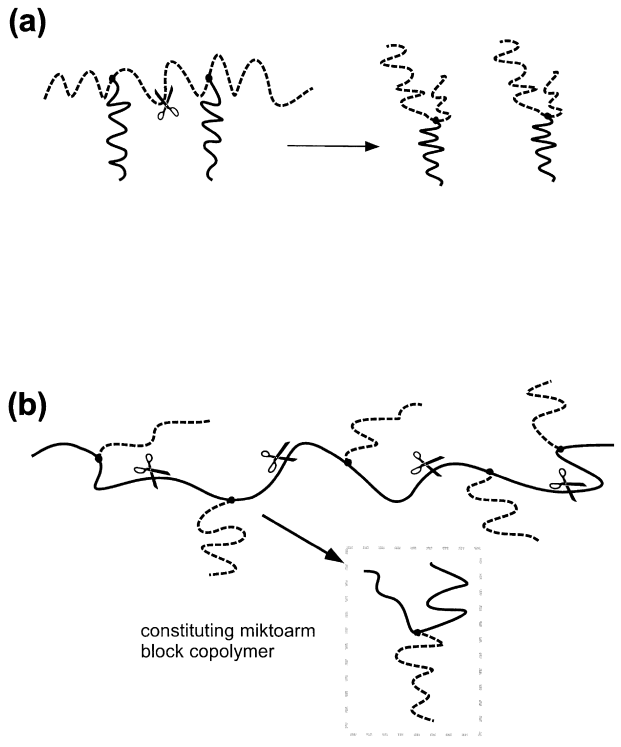

Figure 1 Graft copolymers with constituting *mikto*arm block copolymers: (a) π or (S,I)I′(S,I) double-graft architecture and its constituting asymmetric single-graft block copolymer, (S,I)(1/2I′); and (b) multiple-graft copolymer

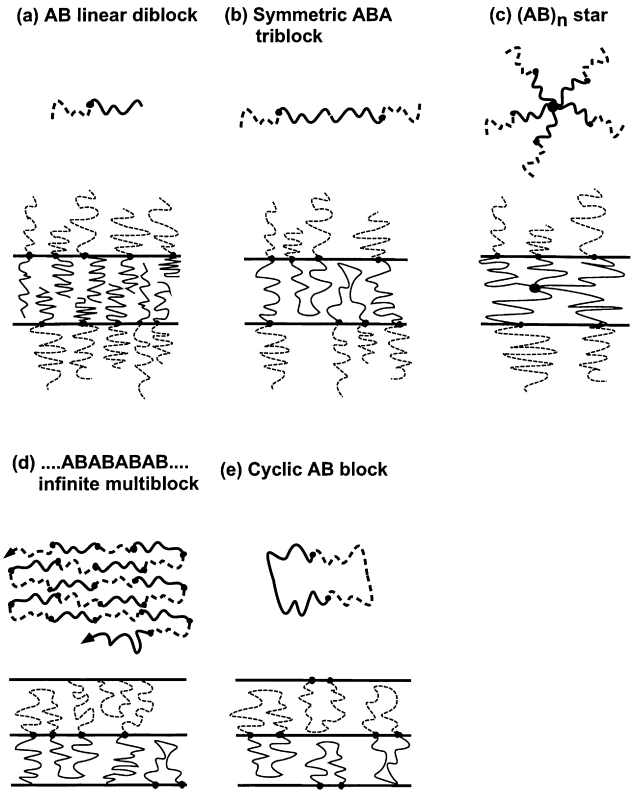

Figure 2 Linear diblock copolymer and copolymers with linear constituting block copolymers: (a) linear diblock copolymer; (b) ABA symmetric triblock copolymer; (c) $(AB)_n$ star block copolymer; (d)…ABAB… infinite multiblock copolymer; and (e) cyclic AB block copolymer

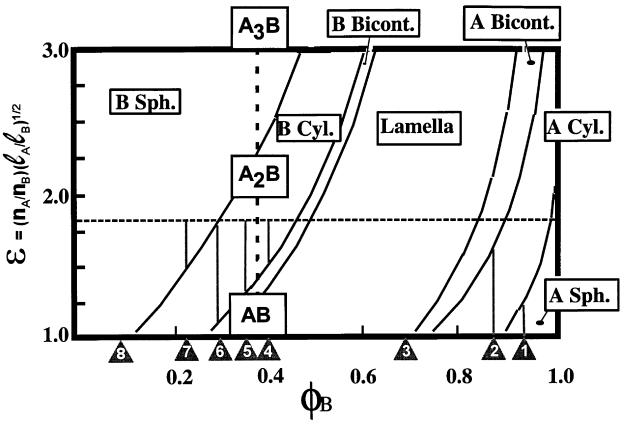

Figure 3 Theoretical phase diagram calculated by Milner. Each triangle represents a specific π sample corresponding to the number within the triangle

$\varepsilon = (n_A/n_B)(l_A/l_B)^{1/2}$. Here (n_A/n_B) is the ratio of arm numbers for the two block types and represents the asymmetry due to the molecular architecture. The factor $(l_A/l_B)^{1/2}$ expresses the conformational asymmetry between the two block materials, and l_i (i = A or B) is the ratio of segment volume to the square of statistical segment length for the *i* block. The value of $(l_A/l_B)^{1/2}$ is characteristic of any opposing pair of block materials. For the polyisoprene–polystyrene (PS–PI) block copolymers used in this study[20,21], $(l_{PS}/l_{PI})^{1/2} \approx 0.89$. The effect of architectural asymmetry results in shifts of the morphological order–order transition lines toward higher volume fractions of the lower arm number component, f_B. Three *corresponding block copolymers*, linear diblock AB, A_2B, and A_3B, are mapped on the dashed vertical line ($f_B = 0.37$) in *Figure 3* as an example. Corresponding block copolymers are defined as block copolymers with different molecular architectures but with the same overall A and B composition and the same total molecular weight. The calculation predicts a lamellar morphology for the linear diblock, a cylindrical morphology for A_2B, and a spherical morphology for A_3B. These morphological differences between corresponding block copolymers are a result solely of differences in molecular architecture. Tselikas *et al.*[26] have recently demonstrated another shift in morphology brought about solely by a change in molecular architecture. A linear, alternating tetrablock copolymer was found to form a lamellar morphology, while the four arm invert star block copolymer of the same composition, formed by joining two such tetrablocks at a junction point in the center of the chains, formed a bicontinuous structure.

Comparing an A_2B block copolymer with a corresponding linear diblock copolymer (2A)B with the same molecule weight and composition, the two short A blocks (*Figure 4b*) are more highly stretched than the single A block (*Figure 4a*) which is twice as long. The higher stretching of the two A arms can be partially alleviated by allowing the interface to curve away from them (*Figure 4c*); thus multiple arms of block type A at a single junction result in an enhanced preference for these arms to remain on the convex side of the interface. This preference causes the shifts of order–order transition lines to higher B block volume fractions in the morphology diagram. Several series of samples with I_2S[20], I_3S[21] and Vergina star[27] (I_8S_8) molecular architecture have been systematically investigated, and all display the effects of molecular architecture on morphology. Although all these experimental studies showed a general agreement with the Milner morphology diagram, there were some minor discrepancies, which indicate that the morphology diagram slightly overestimates the architecturally induced morphological shift, especially at higher volume fractions of the graft block. In a previous study[12], we attributed these discrepancies to a junction point localization effect which was neglected in Milner's calculation. The entropic contribution to free energy resulting from the localization of junction points in the interphase region between domains, which was originally included in the diblock copolymer calculations of Helfand[28–30], was found to become increasingly significant as the number of blocks connected to a junction increases.

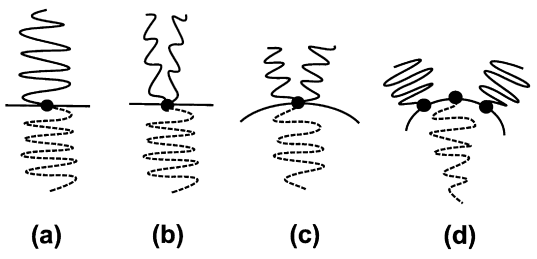

Figure 4 Schematic of A–B junction points on an interface for (a) (2A)B linear diblock copolymer; (b) A_2B single graft block copolymer with a trifunctional branch point at a flat interface; (c) A_2B single graft block copolymer with a trifunctional branch point at a curved interface; and (d) A_2B block copolymer with the approximation of equal spacing between the grafted A blocks. The curvature of the interface, which is exaggerated, represents the shifts of the order–order transition lines toward the higher B volume fraction on the morphology diagram

In the present paper, we report on the morphology of a series of samples with a (S,I)I′(S,I) or π architecture, in which there are two *mikto*arm junction points. As shown in *Figure 1a*, cutting the PI connector (I′) in half gives a *mikto*arm constituting block copolymer with (S,I)(1/2I′) or asymmetric single-graft architecture (ASG). The morphology of a π block copolymer should approximate that of its ASG constituting block copolymer, as long as the molecular weight of the PI connector (I′) is large enough for the two junction points to behave independently. We have reported on the morphologies of a series of samples with ASG architecture in a previous study[31]. The ASG architecture is a more general form of constituting block copolymer with a trifunctional junction point than the symmetric single-graft I_2S materials[20,21], which are constituting block copolymers for H-shaped double-graft block copolymers[12]. In the notation of Olvera de la Cruz and Sanchez[15], τ is defined as the fractional distance along the PI backbone at which the PS graft occurs. As the value of τ increases from 0.0 to 0.5, the ASG architecture changes from a linear diblock to a symmetric simple graft I_2S architecture.

The morphological behaviour of the ASG molecular architecture cannot be predicted directly by Milner's morphology diagram, because the calculation of the ε parameter assumes that all blocks of the same type are of the same molecular weight, i.e. $\tau = 0.5$. In order to generalize the morphology diagram to accommodate asymmetric single-grafts and thus (through the constituting block copolymer mapping) the π architecture, we postulated the following type of relationship[12,32]: $\varepsilon = f(\tau)(l_A/l_B)^{1/2}$. Here $f(\tau)$ represents the asymmetry due to the molecular architecture. The possible form of $f(\tau)$ has been discussed in our previous papers concerning ASG materials, and the current series of π samples will allow us to draw further conclusions regarding this relationship.

EXPERIMENTAL

Synthesis

The synthesis of the π architecture has been published elsewhere[32]. The methods by which the progress of polymerization and linking reactions are monitored and the final products characterized are also discussed in detail in this previous publication. The progress of the polymerizations and linking reactions was monitored by removing samples from the reactors and analyzing them by size exclusion chromatography (SEC), low angle laser light scattering (LALLS) and membrane osmometry (MO).

The molecular characteristics of the polystyrene and polyisoprene arms, polyisoprene connectors and final fractionated π copolymers are given in *Table 1*. The narrow molecular weight distribution found by SEC (RI and UV detectors), the good agreement between the M_n values

for the final products, determined by MO, and the calculated M_n with the equation: $(M_n)_\pi = (M_n)_{PI\ conn} + 2(M_n)_{PI\ arm} + 2(M_n)_{PS\ arm}$ indicate a high molecular and compositional homogeneity. The model character of the π copolymers is also supported by the good agreement between the PS content of the π copolymers, calculated from the M_n (MO) of the precursors and arms, and that found by ^{1}H-NMR and UV-SEC measurement. Finally, the agreement between the values of the specific refractive index increment $(dn/dc)_\pi$, found experimentally (THF, 25°C), and those calculated from the weighted average equation $(dn/dc)_\pi^{calc} = x_S(dn/dc)_{PS} + (1 - x_S)(dn/dc)_{PI}$ is quite good, where x_S is the PS weight fraction, determined by ^{1}H-NMR and UV-SEC. For $(dn/dc)_{PI}$ and $(dn/dc)_{PS}$ we used the average values determined experimentally in THF at 25°C (PI: 0.127 ± 0.001 ml g^{-1}; PS: 0.188 ± 0.001 ml g^{-1}). In those cases where some PI segments are relatively short (i.e., π1 and π2), the connectivity in the π architecture leads to overall PI molecular weights which are still higher than the critical M_n, above which *dn*/*dc* becomes molecular weight independent. This justifies use of the cited homopolymer *dn*/*dc* values for all samples.

Morphological characterization

Solid films approximately 2 mm thick of graft block copolymers were slowly cast from five weight percent polymer solutions in toluene, a nonpreferential solvent. Casting was performed at room temperature, and evaporation of solvent was controlled to form a solid film after 10–14 days. The films were given several more days at room temperature and atmospheric pressure and an additional several days under high vacuum at room temperature in order to remove residual solvent. The samples were then annealed for 1 week under high vacuum at 120°C in order to further promote the approach to an equilibrium structure, and the development of long-range order.

Samples for electron microscopy were microtomed in a Leica Ultracut cryoultramicrotome. Sections approximately 50–100 nm thick were cut with a Diatome diamond knife at a sample temperature of − 110°C and a knife temperature of − 90°C. The sections were stained in OsO_4 vapours for 4 h. Transmission electron microscopy (TEM) was performed using a JEOL 100CX operated at 100 kV accelerating voltage. Small angle neutron scattering (SANS) was performed on beam line NG3 at the Cold Neutron Research Facility of the National Institute of Standards and Technology in Gaithersburg, Maryland. The NG3 instrument uses pinhole collimation of the monochromated beam. Data were recorded with the incident neutron radiation striking the sample parallel to the surface of the cast films at a wavelength of 5 Å. Sample to detector distances (camera lengths) of both 3 and 13 m were used.

RESULTS

TEM images of the π double-graft block copolymer morphologies are shown in *Figures 5–7*, and the SANS results on these materials are shown in *Figure 8*. The SANS results for each sample are displayed as a one-dimensional plot of the natural logarithm of intensity (ln *I*) *versus* scattering vector (**q**), integrated radially from a two-dimensional scattering pattern. We define **q*** as the scattering vector of the Bragg peak with the lowest scattering angle and $\mathbf{q}_n$ as the series of Bragg peaks, in order of increasing scattering angle, beginning with **q***. The ratios of $\mathbf{q}_n/\mathbf{q}^*$ for each peak are indicated in *Figure 8*. The TEM image for sample π1 (94 vol. % PS) in *Figure 5a* shows PI spherical micelles in a PS matrix with little or no discernible long-range order. An intense peak with a long tail is observed in the π1 SANS pattern in *Figure 8*. Possible reflections in the long tail occur at $\mathbf{q}_n/\mathbf{q}^*$ ratios of $\sqrt{2}$ and $\sqrt{3}$. These SANS data are consistent with limited bcc ordering resulting in the 110, 200 and 211 reflections.

Table 1 Molecular characteristics of the π, (S,I)I′(S,I), block copolymers and their component segments*

Sample (τ)	M_n[a] arm PI × 10^3	M_n[a] arm PS × 10^3	M_n[a] con. PI × 10^3	M_n[a] π × 10^3	M_w[b] π × 10^3	(M_w/M_n)[c] π	(dn/dc)[d] π	% wt PS ^{1}H-NMR	% wt PS UV-SEC	% wt PS cal.	% vol PS
π1, (0.28)	4.9[e]	109	3.9[e]	231	245	1.06	0.184	94.9	94.8	94.5	94
π2, (0.38)	8.9[e]	92.1	11.1[e]	212	225	1.06	0.181	88.9	89.7	86.7	87
π3, (0.29)	20.5	70.9	17.1	200	214	1.07	0.171	71.3	71.8	70.8	68
π4, (0.39)	39.4	48.1	50.0	220	236	1.07	0.154	43.1	44.4	43.7	40
π5, (0.36)	37.8	34.6	42.3	181	195	1.08	0.149	37.7	38.3	38.3	34
π6, (0.38)	45.2	34.3	56.0	212	227	1.07	0.145	31.1	33.2	32.4	28
π7, (0.32)	37.2	19.1	33.3	133	147	1.09	0.142	24.0	24.0	26.2	22
π8, (0.35)	65.5	10.8[e]	71.7	235	259	1.10	0.132	8.6	9.9	9.2	8

*From previous work[24]
[a]Membrane osmometry (MO) in toluene at 35°C
[b]Low angle laser light scattering (LALLS) in THF at 25°C
[c]Size exclusion chromatography (SEC) in THF at 30°C
[d]Laser differential refractometry in THF at 25°C (*dn*/*dc*) in ml g^{-1}
[e]Vapour pressure osmometry (VPO) in toluene at 50°C

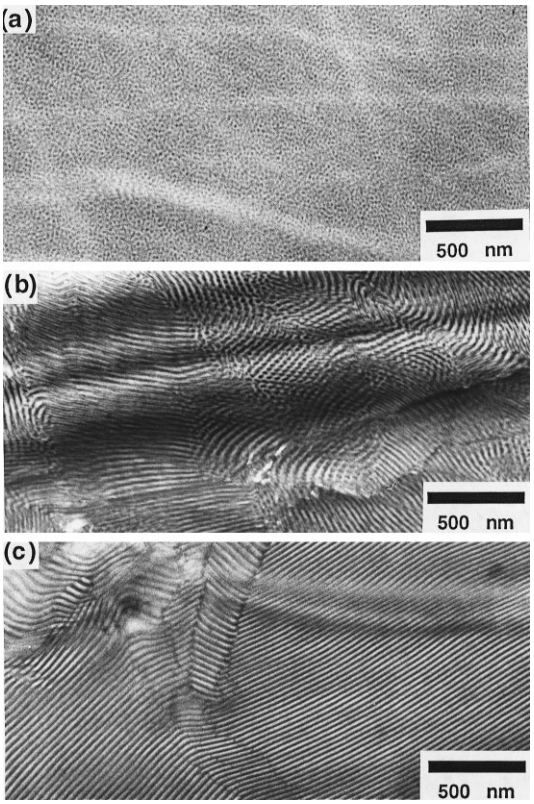

Figure 5 TEM images of (a) the spherical morphology of sample π1; (b) the cylindrical morphology of sample π2; and (c) the lamellar morphology of sample π3

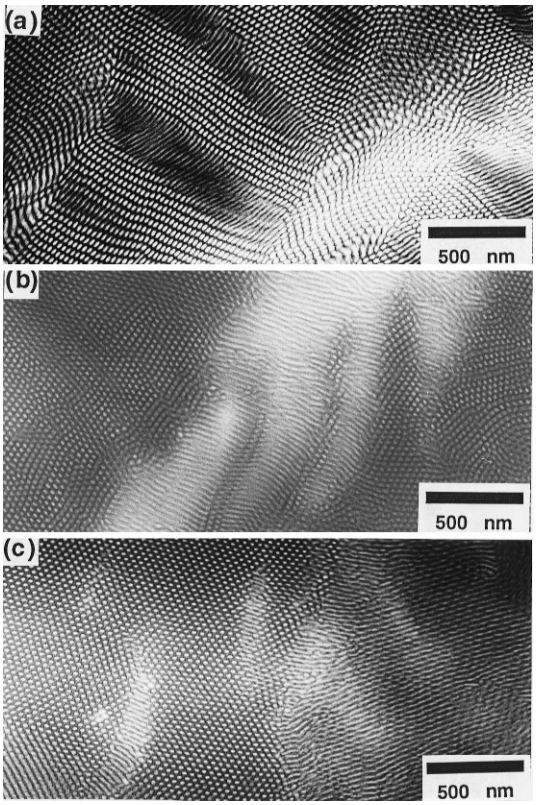

Figure 6 TEM images of the cylindrical morphologies of samples π4 (a), π5 (b) and π6 (c)

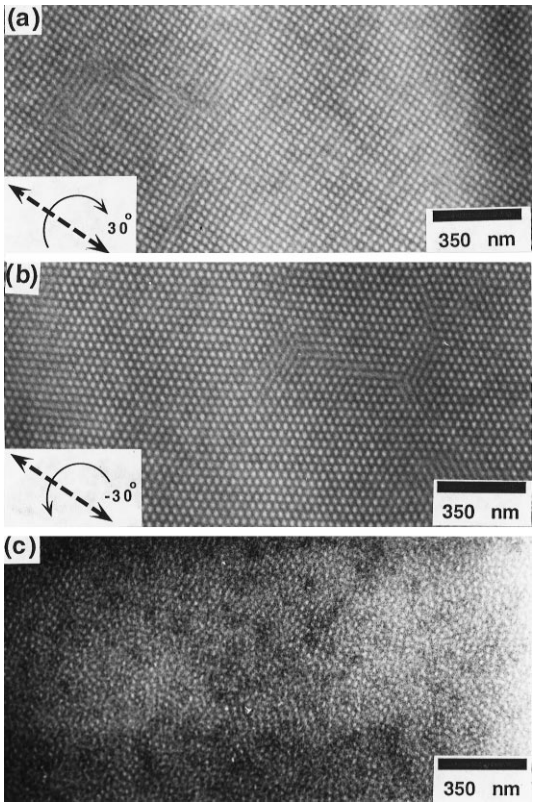

Figure 7 TEM images of the spherical morphologies of samples π7 and π8. The [100] projection (a) and [111] projection (b) from a tilt series on π7 are shown. (c) The spherical morphology of sample π8

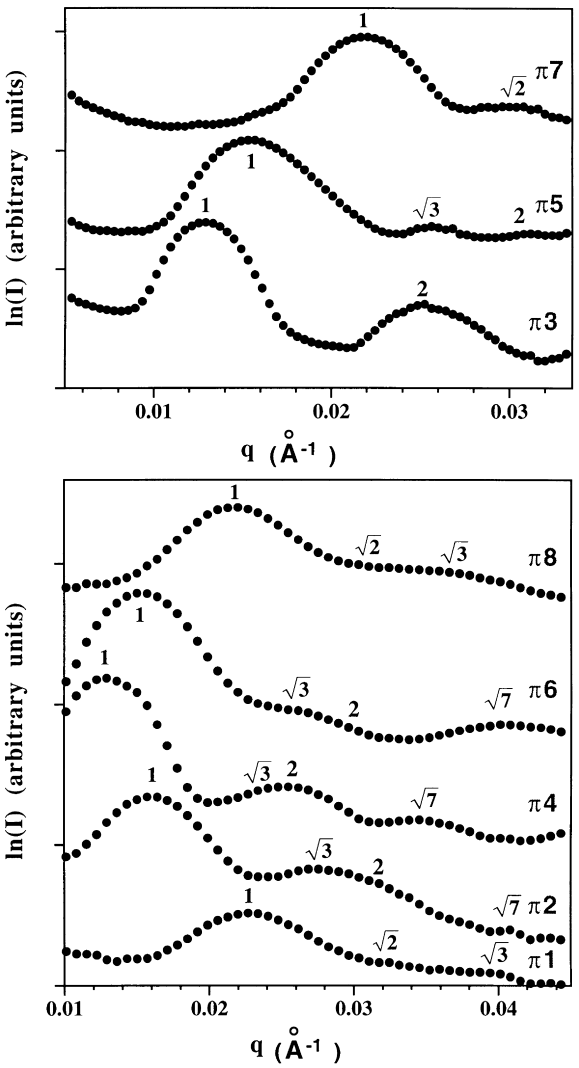

Figure 8 SANS intensity *versus* scattering vector for the π series of samples

The TEM image of π2 (87 vol. % PS), in *Figure 5b*, shows hexagonally packed PI cylinders in a PS matrix. This structure has a small grain size and displays relatively poor long-range order. Both projections parallel and perpendicular to the cylinder axis can be seen among these grains. The SANS ln *I versus* **q** plot for π2 shows three peaks with $\mathbf{q}_n/\mathbf{q}^*$ ratios of 1, √3, and √7, corresponding to the 10, 11, and 21 reflections. The second peak has a very long and rough tail, which may indicate that the 20 reflection, with $\mathbf{q}_n/\mathbf{q}^*$ of 2, is hidden under this peak. Sample π3 (68 vol. % PS), yields a lamellar structure as shown in the TEM image of *Figure 5c*. The ln *I versus* **q** plots in *Figure 8* show two orders of reflection at **q*** and 2**q***.

The TEM images in *Figure 6* for π4 (40 vol. % PS), π5 (34 vol. % PS), and π6 (28 vol % PS) all show hexagonally packed PS cylinders in a PI matrix. Both hexagonal, end-on, and side-on projections of the cylinder structure are visible. The SANS ln *I versus* **q** plots for π4 and π6 show three intense peaks with similar features. The first and third peaks have $\mathbf{q}_n/\mathbf{q}^*$ ratios of 1, and √7 from the 10 and 21 reflections of a hexagonal lattice. The second peak results from the superposition of the 11 and 20 reflections. The ln *I versus* **q** plot for π5 shows three peaks with $\mathbf{q}_n/\mathbf{q}^*$ ratios of 1, √3 and 2, corresponding to the hexagonal 10, 11 and 20 reflections.

Sample π7 forms a cubic array of PS spheres in a matrix of PI. A TEM tilt series in which a relative tilt of

approximately 60° changes the image from a square pattern of projected spheres to a hexagonal pattern, is shown in *Figure 7a* and *Figure 7b*. The axis around which this tilt occurs, indicated by a double-headed dashed arrow, is along a face diagonal of the bcc unit cell. Geometrically, a tilt of 55° about this axis is required to go between the square projection along the [100] direction and the hexagonal projection along the [111] direction. The relative tilt in this experimental series is close enough to the calculated value to provide strong evidence for the bcc structure. There are two peaks shown in the SANS ln *I versus* **q** plot with the $\mathbf{q}_n/\mathbf{q}^*$ ratios of 1 and $\sqrt{2}$, corresponding to the bcc 110 and 200 reflections. The TEM micrograph of π8, *Figure 7c*, shows PS spherical domains dispersed in a PI matrix without noticeable long-range order. Similar to sample π1, the π8 scattering pattern shows one distinguishable peak with a long tail. The tail might be from a superposition of the 200 and 211 reflections, indicating very limited bcc ordering.

DISCUSSION

To compare the characterized morphologies of the π series of samples with Milner's morphology diagram, two assumptions are made as discussed in the Introduction. First, it is assumed that the bridge and loop connections in the interiors of the microphase separated domains can be ignored. Thus the morphology of a π, (S,I)I′(S,I), sample should be same as that of its ASG constituting block copolymer, (S,I)(1/2I′). The τ values for the ASG constituting block copolymers can be simply calculated with the molecular weights of the PI connector and the PI grafts as follows: (1/2I′)/(I + 1/2I′). The calculated τ values for all the π samples are listed in *Table 1*. The second assumption is that a function of τ, $f(\tau)$, can replace the ratio of arm numbers in the molecular asymmetry parameter, ε, used in the calculated morphology diagram[31,32]. This unknown function represents the contribution of the molecular architecture to the molecular asymmetry. The $f(\tau)$ function is necessary because Milner's calculations did not consider *mikto*arm architectures with arms of the same polymer species having different lengths. Thus, the ε values are not known for the ASG constituting block copolymers of the π samples, and we placed a vertical bar for each π sample crossing possible values of ε on the morphology diagram. Since the lateral crowding and additional chain stretching associated with the two chains on one side of the interface in a symmetrically grafted structure ($\tau = 0.5$) should be partially alleviated in the asymmetric simple graft structure, ε should be between 0.89 (linear diblock) and 1.78 (symmetric simple graft architecture, I_2S)[20,21]. That is, the upper and lower limit of the bars plotted on the morphology diagram should be 1.78 and 0.89.

Sample π1, with 94 vol. % PS, displays a morphology of PI spheres in a PS matrix, which is same as that of its corresponding linear diblock copolymer. However, the morphology diagram indicates that its corresponding I_2S block copolymer would produce PI cylinders in a PS matrix. This constrains ε to a small range of values indicated by the vertical bar on the diagram. Sample π2, with 87 vol. % of PS, forms a morphology of PI cylinders in a PS matrix, which is also the same as that of its corresponding linear diblock copolymer but different from that of its corresponding I_2S block copolymer. The allowed range of ε for this sample is also indicated by a bar on the diagram. Sample π3, which forms a lamellar morphology, does not allow us to place any constraints on ε, since at this composition the predicted structure is lamellar across the whole range from 0.89 to 1.78. Samples π4 and π5 both form structures of PS hexagonally packed cylinders in PI matrices. The π architecture induces a morphology shift for these samples from the lamellar structure of their corresponding linear diblock copolymers to a cylindrical structure which they share with their corresponding I_2S block copolymers. The cylinder–bicontinuous order–order transition line provides lower bounds on the two bars specifying the ε ranges for π4 and π5 on the morphology diagram. Sample π6 also displays a cylindrical morphology which is different from either the bicontinuous structure of its corresponding linear diblock copolymer or the spherical structure of its corresponding I_2S block copolymer. Thus, the cylinder–sphere and cylinder–bicontinuous order–order transition boundaries provide both upper and lower bounds on the ε parameter for π6. The π molecular architecture also induces a morphology shift for sample π7 from the cylindrical structure of its corresponding linear diblock copolymer to a spherical structure. This morphology shift provides a lower bound for the bar shown on the diagram. The final sample, π8, also forms a morphology with spherical PS domains in a PI matrix. No bar is shown on the morphology diagram for π8, since its corresponding I_2S and linear diblock copolymers would both also give spherical morphologies.

As discussed in our previous work[31,32], if ε for an asymmetrically grafted molecular architecture is a function of τ, then bounds on this function can be obtained from the bars on *Figure 3*. In the definition of ε, the ratio of the arm numbers is replaced by the function $f(\tau)$: $\varepsilon = f(\tau)(l_A/l_B)^{1/2}$. The function $f(t)$ must be symmetric around $\tau = 0.5$ since the two ends of the PI backbone should be equivalent. The $f(\tau)$ is calculated by dividing ε by $(l_A/l_B)^{1/2}$, which is 0.89 for block copolymers composed of PS and PI. This conversion allows the mapping of the bars in *Figure 3* onto an $f(\tau)$ *versus* τ plot in *Figure 9*. *Figure 9* also includes the results from our previous paper on a series of ASG materials, which are plotted as thinner vertical lines[31]. Each bar on this diagram represents a possible range of values of $f(\tau)$ at each value of τ. When multiple bars have the same τ value, the bars with the lowest upper bound and the highest lower

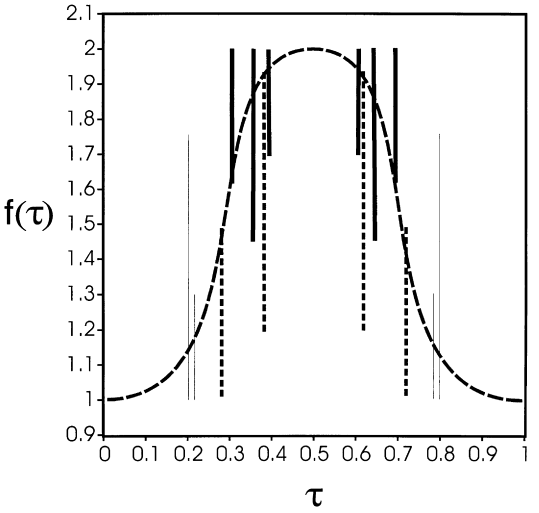

Figure 9 Possible $f(\tau)$ relationship. Bold vertical bars, including the dashed bars, represent allowable ranges of $f(\tau)$ values determined from the π samples in the current study. The thinner vertical bars are from the results on samples with the ASG architecture

bound have been combined to obtain the smallest allowable range. A dashed curve is drawn in *Figure 9* as a qualitative approximation for $f(\tau)$.

The $f(\tau)$ which we have drawn just barely intersects the top of the four dashed bars on the diagram. These bars constrain $f(\tau)$ more than any others and almost make a smooth curve passing through all the bars impossible. The dashed bars are from samples $\pi 1$ ($\tau = 0.28$) and $\pi 2$ ($\tau = 0.38$). These two samples occur in the high graft volume fraction region of the morphology diagram in which the calculation's neglect of junction point localization has the largest effect, causing the order–order transition lines to be shifted a little too far to the right[12]. Owing to this over-shifting effect, the tops of the dashed vertical lines in *Figure 9* should probably be slightly higher. However, the full set of bars on the diagram effectively dictates a bell shape for the $f(\tau)$ function. The bars in *Figure 9* suggest that there may be an inflection point of $f(\tau)$ between $\tau = 0.2$ and $\tau = 0.3$. It indicates that for τ close to zero, the system behaves like a diblock. As τ increases, the behaviour changes in the range $0.20 < \tau < 0.35$ from diblock-like to symmetric simple graft-like behaviour.

The TEM images in *Figures 5–7*, as well as the SANS data in *Figure 8* indicate the rather poor degree of long-range order exhibited by the π double-graft copolymers. Long-range order refers to the degree of perfection of the lattice symmetry, and lattice orientation, and the extent of material over which this symmetry and orientation persists. As one would expect, it is found that the degree of long-range order in graft copolymers decreases with increasing molecular weight and with increasing complexity of molecular architecture. Both the π and the H-shaped double-graft architectures display a significant loss of long-range order when compared with simpler single graft[20] and diblock copolymers. In these double-graft architectures, however, the favoured microphase separated domain shape (sphere, cylinder, bicontinuous, or lamellae) is still clearly distinguishable, even if the domains are not well ordered on a lattice. If the domain shape rather than the lattice symmetry is used as the criterion for mapping onto the Milner morphology diagram, then the constituting block approach may be used to explain the relationship between morphology and graft molecular architecture. Current results (Xenidou M., Gido S. P., and Hadjichristidis N., unpublished) indicate that the domain shape remains distinguishable and can be used to map materials onto the morphology diagram for multiple graft structures with either trifunctional (as in this study) or tetrafunctional branch points and up to five branch points per backbone.

In order to map the morphologies for the π architecture onto the morphology diagram, care has been taken to cast samples from a nonselective solvent, toluene. Results reported previously in our publication on the H architecture indicate that in the case of double-graft materials, selective solvent casting can induce nonequilibrium morphologies which cannot relax to the equilibrium structures during thermal annealing[12]. This is in contrast to the behaviour observed for single-graft materials in which selective solvent cast structures were observed to revert to their equilibrium structures on annealing[33]. The trapping of nonequilibrium structures is a result of the reduced molecular mobility in materials with more complex architecture (multiple graft points) and higher molecular weight. In this sense both reduced long-range order and selective solvent morphology trapping in materials with two (or more) graft points are manifestations of the same effect of molecular architecture on the mobility necessary for effective self-assembly.

CONCLUSIONS

This morphological study of double-graft block copolymers with the π or (S,I)I′(S,I) architecture yields two important results. First the division of complex architectures such as multiple graft structures into *constituting block copolymers* is a valid procedure to aid in understanding the morphological behaviour of these complex molecules. In the case of graft architectures, the constituting block copolymers are produced by considering the complex architecture to be divided in the middle of each loop or bridge within microphase-separated domains. This decomposes the multigraft architecture into component single-graft structures which can then be mapped onto the morphology diagram for *mikto*arm stars calculated by Milner.

The second important result of this study is that the asymmetric single-graft architecture of the constituting block copolymers for the π architectures requires us to generalize the molecular asymmetry parameter, ε, used in the calculated morphology diagram. This generalization is necessary because the Milner calculation was only carried out for symmetrically grafted materials. In the definition of the generalized ε, the ratio of the arm numbers is replaced by the function $f(\tau)$, which represents the contribution to molecular asymmetry resulting from molecular architecture as a function of the fractional location of the graft point, τ, along the backbone.

ACKNOWLEDGEMENTS

Helpful discussions with and experimental assistance from Dr Darrin J. Pochan is acknowledged. J.W.M. and S.P.G. acknowledge funding from the U.S. Army Research Office (ARO) under contract DAAH04-94-G-0245. S.P.G. acknowledges ARO funding through an Army Young Investigator Award DAAH04-95-1-0305. We acknowledge the use of TEM instrumentation in the W. M. Keck Electron Microscopy Laboratory at the University of Massachusetts Amherst, ARO instrumentation funding (DAAH04-95-1-0005), and Central Facility Support from the Materials Research Science and Engineering Center (MRSEC) at the University of Massachusetts Amherst. We also acknowledge the staff of the Cold Neutron Research Facility at NIST for assistance with SANS experiments. Y.P. and N.H. wish to acknowledge the Greek General Secretariat of Research and Technology and the Research Committee of the University of Athens for financial support.

REFERENCES

1. Bi, L.-K. and Fetters, L. J., *Macromolecules*, 1976, **9**, 732.
2. Pennisi, R. W. and Fetters, L. J., *Macromolecules*, 1988, **21**, 1094.
3. Mays, J. W., *Polym. Bull.*, 1990, **23**, 247.
4. Iatrou, H. and Hadjichristidis, N., *Macromolecules*, 1992, **25**, 4649.
5. Bi, L.-K., Fetters, L. J. and Morton, M., *Polym. Prepr. (Am. Chem. Soc. Div. Polym. Chem.)*, 1974, **15**(2), 157.
6. Bi, L.-K. and Fetters, L. J., *Macromolecules*, 1975, **8**, 90.
7. Alward, D. B., Kinning, D. J., Thomas, E. L. and Fetters, L. J., *Macromolecules*, 1986, **19**, 215.
8. Thomas, E. L., Alward, D. B., Kinning, D. J., Martin, D. C., Handlin, D. L. Jr and Fetters, L. J., *Macromolecules*, 1986, **19**, 2197.
9. Watanabe, H., *Macromolecules*, 1995, **28**, 5006.
10. Fredrickson, G. H. and Bates, F. S., *Annu. Rev. Mater. Sci*, 1996, **26**, 501.

11. Gehlsen, M. D., Almdal, K. and Bates, F. S., *Macromolecules*, 1992, **25**, 939.
12. Lee, C., Gido, S. P., Poulos, Y., Hadjichristidis, N., Beck Tan, N., Trevino, S. F. and Mays, J. W., *Journal of Chemical Physics*, 1997, **107**, 6460.
13. Whitmore, M. D. and Vavasour, J. D., *Acta Polymerica*, 1995, **46**, 341.
14. Matsen, M. W. and Schick, M., *Macromolecules*, 1994, **27**, 6761.
15. Olvera de la Cruz, M. and Sanchez, I. C., *Macromolecules*, 1986, **19**, 2501.
16. Matsen, M. W. and Schick, M., *Macromolecules*, 1994, **27**, 7257.
17. Lescanec, R. L., Hajduk, D. A., Kim, G. Y., Gan, Y., Yin, R., Gruner, S. M., Hogen-Esch, T. E. and Thomas, E. L., *Macromolecules*, 1995, **28**, 3485.
18. Marko, J. F., *Macromolecules*, 1993, **26**, 1442.
19. Hadjichristidis, N., Iatrou, H., Behal, S. K., Chludzinski, J. J., Disko, M. M., Garner, R. T., Liang, K. S., Lohse, D. J. and Milner, S. T., *Macromolecules*, 1993, **26**, 5812.
20. Pochan, D. J., Gido, S. P., Pispas, S., Mays, J. W., Ryan, A. J., Fairclough, P. A., Hamley, I. W. and Terrill, N. J., *Macromolecules*, 1996, **29**, 5091.
21. Tselikas, Y., Hadjichristidis, N., Iatrou, H., Liang, K. S. and Lohse, D. J., *Journal of Chemical Physics*, 1996, **105**, 2456.
22. Milner, S. T., *Macromolecules*, 1994, **27**, 2333.
23. Bates, F. S. and Fredrickson, G. H., *Macromolecules*, 1994, **27**, 1065.
24. Matsen, M. W. and Schick, M., *Macromolecules*, 1994, **27**, 4014.
25. Pochan, D. J., Gido, S. P., Zhou, J., Mays, J. W., Whitmore, M. and Ryan, A. J., *Journal of Polymer Science, Polymer Physics*, 1997, **35**, 2629.
26. Tselikas, Y., Hadjichristidis, N., Lescanec, R. L., Honeker, C. C., Wohlgemuth, M. and Thomas, E. L., *Macromolecules*, 1996, **29**, 3390.
27. Beyer, F. L., Gido, S. P., Poulos, Y., Avgeropoulos, A. and Hadjichristidis, N., *Macromolecules*, 1997, **30**, 2373.
28. Helfand, E. and Wasserman, Z. R., *Macromolecules*, 1976, **9**, 879.
29. Helfand, E. and Wasserman, Z. R., *Macromolecules*, 1978, **11**, 960.
30. Helfand, E. and Wasserman, Z. R., *Macromolecules*, 1990, **13**, 994.
31. Lee, C., Gido, S. P., Pitsikalis, M., Mays, J. W., Beck-Tan, N., Trevino, S. F. and Hadjichristidis, N., *Macromolecules 1997. Macromolecules*, 1997, **30**, 3732.
32. Gido, S. P., Lee, C., Pochan, D. J., Pispas, S., Mays, J. W. and Hadjichristidis, N., *Macromolecules*, 1996, **29**, 7022.
33. Pochan, D. J., Gido, S. P., Pispas, S. and Mays, J. W., *Macromolecules*, 1996, **29**, 5099.